research paper

JOURNAL OF APPLIED CRYSTALLOGRAPHY

ISSN 1600-5767

Instrumentation and experimental procedures for robust collection of X-ray diffraction data from protein crystals across physiological temperatures

Tzanko Doukov,[a]*‡ Daniel Herschlag[b,c,d] and Filip Yabukarski[b]*‡

[a]SMB, Stanford Synchrotron Radiation Lightsource, SLAC National Accelerator Laboratory, 2575 Sand Hill Road, Menlo Park, CA 94025, USA, [b]Department of Biochemistry, Stanford University, Stanford, CA 94305, USA, [c]Department of Chemical Engineering, Stanford University, Stanford, CA 94305, USA, and [d]Stanford ChEM-H, Stanford University, Stanford, CA 94305, USA. *Correspondence e-mail: tdoukov@slac.stanford.edu, fyabukar@stanford.edu

Received 24 March 2020
Accepted 8 October 2020

Edited by J. Hajdu, Uppsala University, Sweden and The European Extreme Light Infrastucture, Czech Republic

‡ These authors contributed equally.

Keywords: room temperature; physiological temperature; X-ray crystallography; data collection methods; protein crystals.

Supporting information: this article has supporting information at journals.iucr.org/j

Traditional X-ray diffraction data collected at cryo-temperatures have delivered invaluable insights into the three-dimensional structures of proteins, providing the backbone of structure–function studies. While cryo-cooling mitigates radiation damage, cryo-temperatures can alter protein conformational ensembles and solvent structure. Furthermore, conformational ensembles underlie protein function and energetics, and recent advances in room-temperature X-ray crystallography have delivered conformational heterogeneity information that can be directly related to biological function. Given this capability, the next challenge is to develop a robust and broadly applicable method to collect single-crystal X-ray diffraction data at and above room temperature. This challenge is addressed herein. The approach described provides complete diffraction data sets with total collection times as short as ∼5 s from single protein crystals, dramatically increasing the quantity of data that can be collected within allocated synchrotron beam time. Its applicability was demonstrated by collecting 1.09–1.54 Å resolution data over a temperature range of 293–363 K for proteinase K, thaumatin and lysozyme crystals at BL14-1 at the Stanford Synchrotron Radiation Lightsource. The analyses presented here indicate that the diffraction data are of high quality and do not suffer from excessive dehydration or radiation damage.

1. Introduction

Structures obtained from X-ray diffraction of cryo-cooled protein crystals have arguably provided the most impactful contributions of physics to biology. It is now routine to visualize the fold, intramolecular interactions and binding sites of proteins – information with profound implications for the understanding of protein structure, function and evolution (Berg *et al.*, 2002; Brändén & Tooze, 1999; Fersht, 2017; Ufimtsev & Levitt, 2019; Wlodawer *et al.*, 2008). The thousands of examples of protein structures, along with simplified energetic rules, have led to our current ability to predict structure from sequence for many proteins and to design proteins that form specified folds in many cases (Huang *et al.*, 2016; Kuhlman & Bradley, 2019; Marks *et al.*, 2012).

In contrast, our ability to predict the energetics of protein folding, binding and function is limited. This contrast appears to arise from fundamental principles of physics: free energy, which specifies preferred states and their relative occupancy, is determined from relative energies of states within the protein conformational ensemble. Traditional X-ray crystallography provides structural information at 100 K, but temperatures below the 'glass transition' (generally in the 180–220 K range)

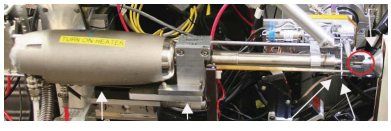

can alter protein conformational heterogeneity, the experimental manifestation of conformational ensembles, and quell function (Fraser *et al.*, 2009; Halle, 2004; Juers & Matthews, 2001; Keedy *et al.*, 2014; Sandalova *et al.*, 1999). Furthermore, and probably of more general importance, traditional X-ray crystallography models provide limited conformational heterogeneity information (Ringe & Petsko, 1985; Petsko, 1996; Furnham *et al.*, 2006). Underscoring the need for in-depth detailed information about conformational heterogeneity, there has been considerable discussion about the tuning of protein motions and conformational heterogeneity to suit physiological temperatures (Feller, 2010; Fields *et al.*, 2015; Siddiqui & Cavicchioli, 2006; Elias *et al.*, 2014).

Unlocking the potential of X-ray crystallography to provide conformational heterogeneity information at physiological temperatures that can be more directly related to native conformational ensembles, energetics and function requires an ability to routinely obtain high-quality X-ray diffraction data at physiological temperatures. While historically X-ray diffraction data have exclusively been collected at room temperature (RT), cryo-cooling of crystals allowed substantial improvements in data quality, speed of data collection and amount of information that could be obtained from a single crystal (Hope, 1988), and cryo-temperature data collection quickly overtook protein X-ray crystallography. Nevertheless, developments in instrumentation for RT data collection continued (*e.g.* Sjögren *et al.*, 2002). Recent advances in X-ray sources, optics and detectors have led to a renaissance in RT X-ray crystallography data collection, and parallel method development has enabled conformational heterogeneity information to be obtained from the RT diffraction data and to be related to function (Fraser *et al.*, 2011, 2009; Keedy *et al.*, 2014, 2018; van den Bedem *et al.*, 2009; Lang *et al.*, 2010).

Although technical and methodological progress in collecting higher temperature data has demonstrated that physiological temperature data collection is possible – *e.g.* early work developed a method to enable data collection at temperatures up to 303 K and in more recent work X-ray data were collected up to 353 K – these experiments remain challenging (Sjögren *et al.*, 2002; Rajendran *et al.*, 2011). Strategies for routinely obtaining these data are needed to expand the usage and thus impact of RT X-ray crystallography. In addition, the ability to obtain data across the range of physiological temperatures would allow models for the evolutionary tuning of protein function and the origins of protein conformational heterogeneity to be tested and new models to be developed. Ultimately, with sufficient data, these approaches, coupled with computational advances, will extend our abilities from predicting structures to predicting conformational ensembles, the latter being related to the energy of the system via the laws of statistical mechanics.

Here we present a robust and potentially broadly applicable method for efficiently collecting single-crystal X-ray diffraction data at and above room temperature at synchrotron beamlines. We present the technical aspect of the instrumentation and data collection strategy that have allowed us to obtain single-crystal X-ray diffraction data at beamline 14-1 (BL 14-1) at the Stanford Synchrotron Radiation Lightsource (SSRL) and which can be generalized to other beamlines. With this approach, we can take full advantage of prior technical developments (*i.e.* brighter beamlines and fast detectors) and obtain complete diffraction data sets of high quality with total collection times as short as ∼5 s, allowing for large quantities of data to be collected during allocated beam time at experimental X-ray crystallography stations.

2. Experimental

2.1. Obtaining crystals for X-ray diffraction at and above room temperature

Tritirachium album proteinase K (catalog No. P2308), *Thaumatococcus daniellii* thaumatin (catalog No. T7638) and hen egg lysozyme (catalog No. L4919) were purchased from Sigma and crystallized at room temperature as previously described (https://www.moleculardimensions.com/products/ready-to-grow-crystallization-kit) using hanging-drop (proteinase K and lysozyme) and sitting-drop (thaumatin) setups.

Crystals are more sensitive to radiation damage at room temperatures than at cryo-temperatures (see below), and the diffractive contribution from a unit cell is destroyed by a lower number of absorbed photons than at cryo-temperatures (Garman & Weik, 2017; Garman & Owen, 2006; Nave & Garman, 2005; Roedig *et al.*, 2016; Southworth-Davies *et al.*, 2007; Warkentin *et al.*, 2011; Warkentin & Thorne, 2010); thus, collecting X-ray diffraction data at and above room temperature to resolutions approaching those available from cryo-cooled crystals requires a larger number of unit cells (and a correspondingly larger crystal). Our experience suggested that crystals of dimensions 0.3 mm or larger are optimal, but the approach could be used to collect diffraction data from smaller crystals, generally at the expense of resolution, as expected. To maximize diffraction intensity while minimizing the number of absorbed photons per unit cell, we matched the horizontal beam sizes (200–300 µm) to fit within the largest crystal dimension which is mounted and placed on the goniometer rotation axis (see Table S6 of the supporting information).

2.2. Achieving high-temperature capabilities and temperature control

To enable high-temperature data collection at SSRL BL 14-1, an Oxford Cryosystems Cryostream 800 model N_2 heater/cooler with a temperature range of 80–400 K (temperature stability of 0.1 K) was installed. The nozzle was aligned coaxially to the sample holding pin [Fig. 1(*a*)], and the temperature at the crystal position was confirmed with a type J thermocouple on Omega HH23 microprocessor thermometer. Because the physical properties of protein crystals deteriorate with high-temperature exposure, we used a crystal annealer in 'sample protective mode' to control the crystal exposure to the N_2 stream as follows: After the desired (high) temperature of the N_2 stream is achieved and prior to mounting the sample in the N_2 stream, the annealer paddle is placed in the 'closed'

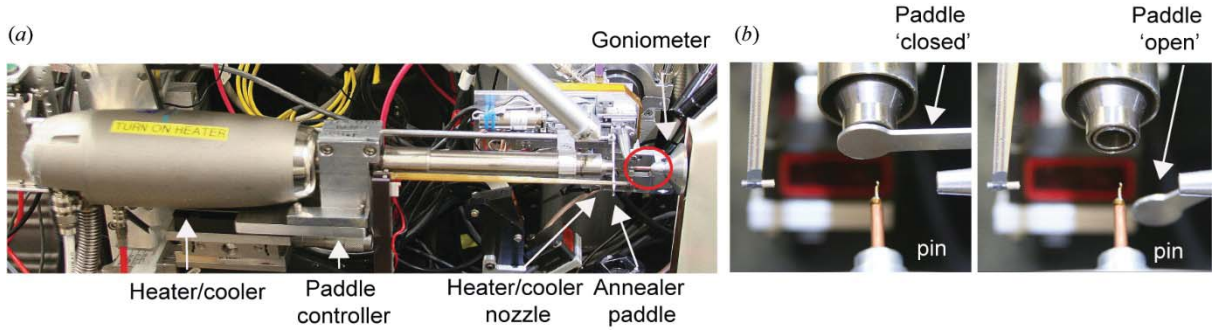

Figure 1
Experimental setup for X-ray diffraction data collection at and above room temperature. (*a*) The Oxford Cryosystems heater/cooler mounted on the annealer device working in 'sample protective mode' during the preparation stages. The pin holding the sample (circled in red) is co-axially aligned with the heater/cooler nozzle. The X-ray beam and the X-ray detector are orthogonal to the sample/heater line. (*b*) The annealer paddle blocks N_2 in the 'closed' position (left) and allows the N_2 gas to reach the crystal mounted on the pin in the 'open' position (right).

position to prevent the gas flow from reaching the sample and heating it unnecessarily during experimental setup [Fig. 1(*b*), left; *i.e.* crystal mounting and centering, closing the experimental hutch, entering the experimental parameters into the control software]. After the sample is mounted, the annealer paddle is moved to the 'open' position [Fig. 1(*b*), right] via the beamline control software *BluIce* (McPhillips *et al.*, 2002) and data collection is initiated after a short temperature equilibration delay. Control kinetic measurements showed that a J thermocouple moved from room temperature (∼293 K) to a 363 K N_2 stream (the highest temperature used in this work) was at 360.5 K, within 5% of the desired temperature, in less than 10 s (not shown). We used this equilibration time prior to data collection (see below). The diffraction data obtained provided additional independent evidence that the crystal temperature increased with increasing N_2 gas temperature (see Fig. 2 in the *Results* section).

2.3. Absorbed X-ray dose

At cryo-temperatures, a dose of ∼20 MGy was proposed as a limit expected to halve the diffraction intensity of protein crystals; later experiments using ferritin crystals estimated that a dose of ∼43 MGy halved the diffraction intensity and ∼30 MGy was proposed as an experimental limit (Henderson & Clarke, 1990; Owen *et al.*, 2006), while additional work suggested that X-ray doses of 10 MGy could be expected to decrease diffraction resolution by 1 Å (Howells *et al.*, 2009). Protein crystals exhibit a range of increased sensitivities to radiation damage at room temperature, typically increased 50–100 times relative to cryo-temperatures but by some estimates up to 300 times (Roedig *et al.*, 2016; Southworth-Davies *et al.*, 2007; Warkentin *et al.*, 2011; Warkentin & Thorne, 2010). We used doses 200–500-fold lower than the 10 MGy limit, corresponding to total absorbed maximum doses of about 20–50 kGy for data sets of 180° total rotation. This dose range is also within the 380 kGy dose recently proposed as a guide to limit global radiation damage, based on serial synchrotron X-ray crystallography experiments on lysozyme crystals (de la Mora *et al.*, 2020). Crystals suffer radiation damage even with such low doses, but recent work has suggested that the conformational heterogeneity in protein crystals at room temperature is not dominated by radiation damage and that specific damage does not occur appreciably before the diffraction resolution deteriorates (*i.e.* crystal diffraction is often lost before specific damage becomes significant), in contrast to observations from cryo data sets (Gotthard *et al.*, 2019; Russi *et al.*, 2017; Roedig *et al.*, 2016). While previous work provides evidence for and against dose-rate (absorbed X-ray dose per unit of time) effects at room temperature, with the magnitude of dose-rate effects and the dose range at which these effects occur being debated, an increasing amount of evidence suggests that, for a given total X-ray dose, higher dose rates can extend crystal lifetimes allowing more data to be collected from a single crystal (Southworth-Davies *et al.*, 2007; Warkentin *et al.*, 2012; Owen *et al.*, 2012, 2014); we therefore used dose rates of ∼1–4 kGy s^{-1}, which were at the high end of the dose rates possible at BL14-1 and compatible with our experimental setup (see Tables 1 and S1).

2.4. Minimizing time-dependent X-ray damage at room temperature

At room temperature, the X-ray-induced damage has a time component, such that damage continues even after the X-ray source has been turned off (Blundell & Johnson, 1976; Warkentin *et al.*, 2011). In particular, this can happen when, after collection of a few test diffraction images, the crystal is left on the goniometer while the experiment is set up (usually on the order of minutes) and when the shutter is closed after collecting a frame on a CCD detector and before it is opened again for the next frame ('readout time', typically from a few seconds to dozens of seconds between frames).

To circumvent these limitations and reduce time-dependent X-ray damage and associated diffraction intensity decay, we eliminated the initial X-ray test exposures that are traditionally used for cryo data collection (Dauter, 1999). Instead, we implemented a fast data collection strategy in which a diffraction data set can be collected immediately following thermal equilibration of the crystal. A complete data set can be obtained for most protein crystal types and initial crystal orientations from 180° (or less) total rotation (Dauter, 1999,

Table 1
Diffraction statistics.

Proteinase K, thaumatin and lysozyme crystal diffraction statistics are reported for data sets of 100° total rotation, which were sufficient for high completeness. Values in parentheses are for the highest-resolution shells. Unit-cell parameters were obtained using images from the entire 100°. All statistics were obtained from *Aimless* (Evans & Murshudov, 2013), with the exception of Wilson *B* factor, ISa and $CC_{1/2}$, which were obtained from *XSCALE* (Kabsch, 2010). Absorbed X-ray doses were estimated using the program *RADDOSE* (version 2; Paithankar *et al.*, 2009) and input parameters from Table S6 [also see Table S6 for X-ray dose estimates from *RADDOSE-3D* (Zeldin *et al.*, 2013; Bury *et al.*, 2018)]. Statistics for data sets used in Fig. 2 are reported in Table S1.

	Proteinase K					Lysozyme		Thaumatin	
Temperature (K)	293	333	343	353	363	293	323	293	313
Wavelength (Å)	0.95369	1.03316	1.03316	1.03316	1.12709	1.03316	1.03316	1.03316	1.03316
Resolution range (Å)	35.05–1.09 (1.11–1.09)	35.21–1.22 (1.24–1.22)	35.43–1.21 (1.23–1.21)	34.18–1.29 (1.31–1.29)	35.58–1.54 (1.57–1.54)	33.54–1.16 (1.18–1.16)	35.09–1.59 (1.62–1.59)	38.32–1.39 (1.41–1.39)	38.43–1.50 (1.53–1.50)
Dose (kGy)	10	10	28	30	32	15	12	15	18
Collection time (s)	20	10	10	10	10	5	5	5	5
Dose rate (kGy s^{-1})†	0.5	1.0	2.8	3.0	3.2	3.0	2.4	3.0	3.6
Space group	$P4_32_12$	$P4_32_12$	$P4_32_12$	$P4_32_12$	$P4_32_12$	$P4_32_12$	$P4_32_12$	$P4_12_12$	$P4_12_12$
Unit-cell dimensions (Å, °)	67.91	68.07	68.40	68.36	68.46	77.82	78.46	58.95	59.19
	67.91	68.07	68.40	68.36	68.46	77.82	78.46	58.95	59.19
	102.46	103.28	104.11	104.04	104.97	37.17	37.27	151.30	151.59
	90.00	90.00	90.00	90.00	90.00	90.00	90.00	90.00	90.00
	90.00	90.00	90.00	90.00	90.00	90.00	90.00	90.00	90.00
	90.00	90.00	90.00	90.00	90.00	90.00	90.00	90.00	90.00
Total reflections	718 902 (31 402)	517 210 (23 196)	514 204 (21 196)	448 926 (18 236)	265 848 (12 015)	282 472 (12 570)	116 775 (5260)	399 610 (19 620)	320 196 (15 156)
Multiplicity	7.2 (6.4)	7.1 (6.6)	6.9 (5.9)	7.2 (6.1)	7.1 (6.6)	7.6 (7.5)	7.3 (6.8)	7.3 (7.4)	7.3 (7.1)
Mosaicity (°)	0.08	0.21	0.43	0.28	0.46	0.11	0.16	0.08	0.09
Completeness (%)	100 (99.9)	99.8 (99.7)	98.7 (97.6)	99.8 (98.6)	99.6 (98.5)	93.5 (86.2)	99.3 (98.6)	100 (99.6)	99.6 (97.9)
Mean $I/\sigma(I)$	7.8 (0.7)	8.5 (0.7)	5.9 (0.6)	7.7 (0.8)	6.2 (0.6)	13.4 (0.7)	9.9 (0.7)	11.1 (0.6)	9.9 (0.7)
Wilson *B* factor ($Å^2$)	13.7	19.6	19.5	21.9	31.6	20.4	32.0	26.8	30.6
R_{merge}	0.12 (2.58)	0.13 (3.57)	0.13 (3.07)	0.13 (3.07)	0.14 (3.31)	0.06 (3.06)	0.09 (2.58)	0.08 (3.34)	0.09 (2.92)
R_{pim}	0.05 (1.09)	0.05 (1.53)	0.05 (1.32)	0.05 (1.31)	0.06 (1.39)	0.02 (1.17)	0.04 (1.03)	0.03 (1.31)	0.04 (1.15)
$CC_{1/2}$	100 (36.6)	100 (30.0)	100 (30.3)	100 (33.1)	100 (31.6)	100 (30.9)	100 (31.0)	100 (32.6)	100 (34.6)
ISa	24.3	27.7	35.1	27.4	21.8	32.8	25.5	23.1	18.2

† The Eiger 16M readout time between frames is 3 µs (Casanas *et al.*, 2016), which corresponds to a 300 µs total readout time for a complete data set of 100 images. This is negligible relative to the 5–20 s total collection time.

2017). The tetragonal symmetry of the crystals used in this work allowed us to obtain complete and high multiplicity data sets from only 100° of total rotation (Tables 1 and S1); 180° of total rotation can be readily collected using the same approach by simply collecting 1.8 times more data and would provide similarly complete (but with less multiplicity) data sets even for the least symmetric crystals. To further reduce time-dependent X-ray damage and minimize the total data collection time, we used rotation images of 1° with exposure times of 0.05–0.2 s per image, allowing a complete data set to be collected within ∼3–36 s, depending on the symmetry of the crystal (Dauter, 1999, 2017). The 0.05–0.2 s (20–5 Hz) exposure times were enabled by the use of high-frequency-frame-rate photon counting detectors (the Eiger 16M detector was used in this work; the 0.05–0.2 s exposure times enable the use of both the Eiger 16M and Pilatus 6M detectors, expanding the applicability of the approach to a larger number of beamlines), with the X-ray shutter closing and opening after the recording of each frame eliminated (*i.e.* 'shutterless' mode) to further reduce the total experimental time and the time-dependent X-ray damage (Brönnimann *et al.*, 2003). In our experiments, the full potential of the Eiger 16M detector (133 Hz) was not achieved owing to current flux limitations at BL14-1 (1.7×10^{11} photons s^{-1} through a 0.2 by 0.08 mm aperture and 500 mA ring current at 10.5 keV). Careful evaluation of the hardware and software capabilities will be required if higher rotational speeds and data collection frequencies are to be routinely used for collecting high-quality data (Diederichs, 2010; Casanas *et al.*, 2016).

The goal of the approach herein is to collect high-quality complete data sets at and above room temperature. To increase the likelihood of success in collecting high-quality diffraction data for a given project, a few crystals of similar size and with similar diffraction properties are required and the crystals need to be prepared in a standardized manner for data collection (see Section 2.5). Slight adjustments in the experimental setup may be needed and implemented (see below), but our experience suggests that uniform work practices increase the success rate. To collect high-quality complete data sets at and above room temperature, we adjusted the experimental parameters to obtain data sets with absorbed maximum doses on the order of 20–50 kGy. Because the total X-ray dose absorbed by a crystal during diffraction data collection directly depends on the experimental parameters (beam intensity, beam size, beam FWHM and collimation, rotation range, and collection frequency), these parameters need to be set prior to data collection to achieve the desired dose. To reduce time-dependent radiation damage effects, the exposure time per image should be short (0.05–0.2 s herein or faster at brighter beamlines) and per-image rotations were set to 1°. The beam intensity to achieve a desired dose can be estimated using the program *RADDOSE*, which would also

require information about the crystal, unit-cell size, and solvent and protein content, among others, and we used *RADDOSE* programs (Paithankar *et al.*, 2009; Zeldin *et al.*, 2013; Bury *et al.*, 2018) to estimate absorbed doses (see Tables 1, S1 and S6). While such dose estimation could be used to directly establish parameters for data collection, in practice we find that using a test crystal diffraction together with initial maximum dose estimates allows us to adjust experimental parameters as needed to collect within the 20–50 kGy range. While twofold X-ray dose over- or underestimation will generally not significantly impact data collection and quality (and there appears to be a twofold uncertainty associated with estimates in general; Holton, 2009), severe overestimation or underestimation of the dose will lead to weak, suboptimal diffraction or excessive damage and incomplete diffraction data sets, respectively, outcomes that can be quickly detected as the diffraction data are analyzed.

2.5. Preparing crystals for data collection

Immediately prior to data collection, the outer layer of the crystal's aqueous mother liquor was exchanged with an inert oil (paratone-N) in the following way: The drop containing the crystals was completely covered with an excess of the paratone-N oil to prevent crystals in the drop from dehydrating (Hope, 1988). Within the drop, each crystal used for data collection was transferred from the mother liquor to the oil while the aqueous layer was stripped (Hope, 1988). Owing to its high viscosity and hydrophobicity, paratone-N acts as an immiscible barrier for water and significantly reduces evaporation (Hope, 1988, 1990; Pflugrath, 2015). Inside an oil drop the aqueous layer on the crystal surface was removed with a nylon loop and the oil-covered crystals were mounted on Dual-Thickness MicroLoops LD and MicroGrippers loops (Mitegen). Excess oil was removed until only a thin coating remained, as any material in the beam would increase the background scattering. Preparing crystals for data collection by exchanging the crystal's mother liquor with oil is straightforward, but achieving the best results will require practice, which we recommend. A short movie outlining the main steps can be found as an online supplemental file. The pins were mounted on the goniometer for thermal equilibration followed by data collection (see Section 2.2).

Several other approaches for collecting X-ray diffraction data from single crystals have been applied to collect data at room temperature, including various types of capillaries and humidity control devices (Skrzypczak-Jankun *et al.*, 1996; Kiefersauer *et al.*, 2000; Sjögren *et al.*, 2002; Sanchez-Weatherby *et al.*, 2009). These approaches could potentially be adapted for data collection at temperatures above room temperature, but data collection using capillaries would require careful evaluation of the physical properties of the capillaries (and seals) at higher temperatures. To our knowledge, currently available humidity control devices have not been demonstrated to allow data collection above 303 K (Sjögren *et al.*, 2002). In addition to allowing for high-temperature data collection (up to 363 K in this work), exchanging crystals with an inert oil also eliminates the risk of potential irreproducible crystal dehydration by exposing the crystal to air, which can occur when crystals are prepared for data collection using various types of capillaries. Lastly, in the exchange with oil approach, the entire drop is covered with oil, minimizing mother liquor evaporation, which protects all crystals in the drop from dehydration and allows the crystals to be utilized uniformly.

2.6. Diffraction data processing

All diffraction data sets were processed using the *XDS* package (Kabsch, 2010) and the programs *Pointless* (Evans, 2006) and *Aimless* (Evans & Murshudov, 2013), as implemented in the *autoxds* in-house processing script at SSRL (https://smb.slac.stanford.edu/facilities/software/xds/).

3. Results

Typically, the goal of X-ray diffraction experiments at and above room temperature is to obtain information about protein conformational heterogeneity and solvent structure for proteins whose overall structure is known (Dunlop *et al.*, 2005; Fischer *et al.*, 2015; Keedy *et al.*, 2014, 2015; Thomaston *et al.*, 2017; Woldeyes *et al.*, 2014). Therefore, the main requirements for data sets obtained across physiological temperatures are high resolution and full completeness of the diffraction data, and we have developed the experimental approach herein accordingly.

To evaluate our experimental approach, we collected data from proteinase K, thaumatin and lysozyme crystals. We obtained single-crystal X-ray diffraction data sets at and above room temperature with estimated absorbed maximum doses of about 10–30 kGy (Tables 1, S1 and S6). All data sets were of outstanding quality, as shown by the very high resolutions and excellent diffraction statistics (Tables 1 and S1). The maximum temperature of data collection was limited only by the physical stability of the crystals at the desired temperature (see below).

For proteinase K, we could obtain complete high-resolution diffraction data sets up to 363 K, and the highest temperatures for thaumatin and lysozyme were 313 and 323 K, respectively (Tables 1 and S1); higher temperatures caused abrupt loss of diffraction. Previous studies in which X-ray diffraction data sets were collected at increasing temperatures reported expansion of crystal unit cells with temperature (Keedy *et al.*, 2015; Kurinov & Harrison, 1995; Tilton *et al.*, 1992). To determine if similar unit-cell thermal expansion occurs, we collected additional data sets for proteinase K crystals within the 293–363 K temperature range, using several crystals at each temperature and collecting an independent and complete data set from each crystal (Tables 1 and S1). Fig. 2(*a*) shows that the average unit cell expands with temperature, consistent with previous observations, and suggesting that the desired temperature has been achieved. The observed slope of 0.3 indicates that the proteinase K unit cell expands at a rate of 300 Å^3 K^{-1}, and we observed slopes of 270 and 140 Å^3 K^{-1} for thaumatin and lysozyme, respectively [Fig. 2(*b*)]. In

contrast to the observed volume increase with increasing temperature, excessive dehydration of protein crystals has been shown to correlate with large decreases in unit-cell volume ($V_{\text{unit cell}}$) (Atakisi *et al.*, 2018). To determine if dehydration occurred during our data collection, we calculated $V_{\text{unit cell}}$ from different stages of the experiments. For the proteinase K temperature series, we compared mean volumes from independent data sets, each collected from independent crystals. To evaluate the extent of changes in $V_{\text{unit cell}}$ during data collection, we compared $V_{\text{unit cell}}$ calculated from images 1–10 and 91–100 from each data set (the first and last 10° from each data set, respectively). To evaluate if unit-cell changes have occurred after collection of 360° of total rotations from each crystal and compare $V_{\text{unit cell}}$ obtained from the same crystal orientation, we also compared the $V_{\text{unit cell}}$ values obtained from images 1–10 and 361–370. Fig. 2(*b*) shows that the $V_{\text{unit cell}}$ values from images 1–10 from each data set (white bars) are similar to the $V_{\text{unit cell}}$ values either from images 91–100 from each data set (gray bars) or from images 361–370 (black bars). The small variations in $V_{\text{unit cell}}$ are consistent with the previously estimated ∼0.2% uncertainties in the determination of unit-cell dimensions (Dauter & Wlodawer, 2015). These observations suggest that no significant dehydration occurred during data collection.

Fig. 2(*c*) shows decreasing resolution with temperature for proteinase K crystals, with a slope of 0.005 Å K^{-1} and still high resolution of 1.54 Å at 363 K; similar decreases in resolution are observed for thaumatin and lysozyme (Table 1). Because all proteinase K data sets were obtained with similar data collection parameters, from several independent crystals for each temperature, and from crystals with similar size and shape, it is unlikely that the observed dependence is fortuitous and caused by random crystal-to-crystal variation.

Several scenarios could account for the decrease of resolution with temperature. Diffraction resolution decay could be caused by increased sensitivity to radiation damage with temperature, such that crystal diffraction decays faster at higher temperatures (a significant increase of sensitivity at room temperature relative to cryo-temperature is consistent with the activation of solvent-coupled diffusive damage processes (*e.g.* increased diffusion of radicals) [see Warkentin *et al.* (2011, 2012), Garman & Weik (2017), Garman (2010) and references therein]. Alternatively or in addition, the decay in diffraction resolution could be caused by increased crystal disorder with increasing temperature. If this were the case then we would expect to see a clear trend of increasing crystal mosaicity with increasing temperature. Fig. 2(*d*) shows such a clear trend in increasing mosaicity with temperature, with a slope of 0.005° K^{-1}, identical to the slope of 0.005 Å K^{-1} observed in Fig. 2(*c*). This observation supports a direct link between mosaicity and resolution and suggests that the decrease in resolution with temperature is caused by increasing crystal disorder, as captured by mosaicity [we also note that increased mosaicity has been observed with increasing radiation damage; *e.g.* see Garman (2010)]. Increased crystal disorder could originate from increasing protein conformational heterogeneity within the crystal unit cell. Alternatively, the increased crystal disorder could be

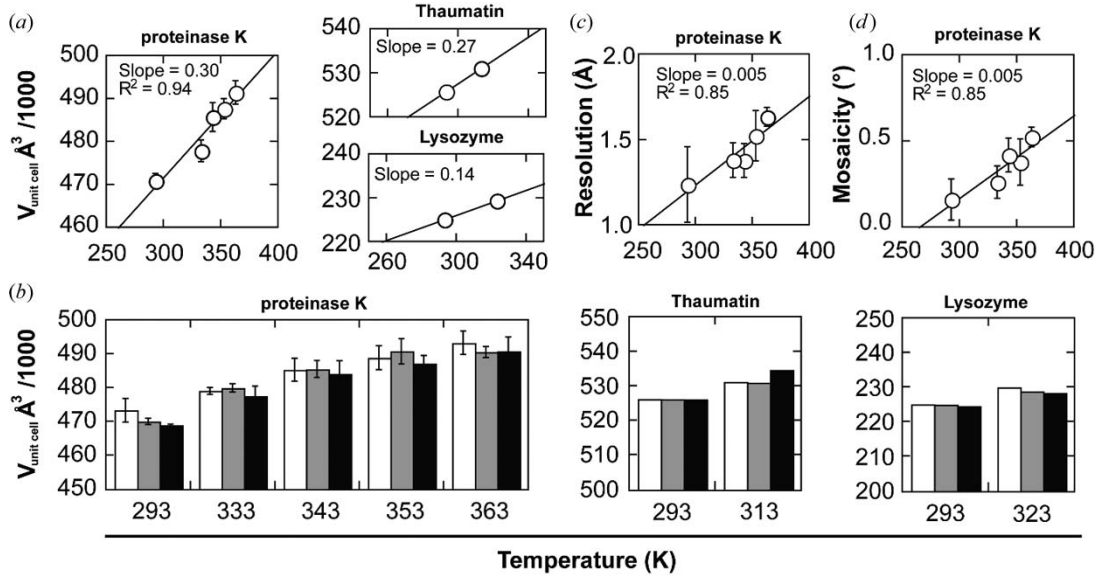

Figure 2
Unit-cell volume, resolution and mosaicity analysis. (*a*) The proteinase K (left), thaumatin (right, top) and lysozyme (right, bottom) unit-cell volume ($V_{\text{unit cell}}$) increases with increasing temperature. For proteinase K, the mean $V_{\text{unit cell}}$ and associated standard deviations from independent data sets were obtained from three (293 K) and four (333–363 K) independent crystals at each temperature. For thaumatin and lysozyme, $V_{\text{unit cell}}$ is obtained from a single crystal at each temperature. (*b*) For proteinase K (left), thaumatin (middle) and lysozyme (right), $V_{\text{unit cell}}$ does not change significantly during data collection. For proteinase K, the mean $V_{\text{unit cell}}$ and associated standard deviations were obtained from images 1–10 (white bars), from images 91–100 (gray bars) and from images 361–370 (black bars) (same crystal orientation as images 1–10 but after a complete 360° rotation during which the crystal was exposed to X-rays) for the data sets in (*a*). For thaumatin and lysozyme, $V_{\text{unit cell}}$ was obtained from a single crystal at each temperature. (*c*) (Top) The proteinase K average data set resolution (cut-off $\simeq 0.3\,CC_{1/2}$) decreases with increasing temperature. (*d*) (Top) The proteinase K average data set mosaicity (images 1–10, 2.0 Å resolution cut-off) increases with increasing temperature. (Bottom) Mean resolutions (*c*) and mosaicities (*d*) and associated standard deviations for data sets in (*a*). See Tables S2–S5 for values used in these plots.

independent of protein conformational heterogeneity. Future work will test this former model by evaluating proteinase K motion with increasing temperature.

4. Discussion and conclusions

A complete quantitative and predictive understanding of biology requires an ability to predict the energetics of protein folding, ligand binding and function. While traditional X-ray crystallography structures have been and remain invaluable in biology and medicine, they do not provide the conformational ensemble information needed to relate structure to energetics. Recent advances in room-temperature X-ray crystallography have demonstrated the ability to obtain ensemble information and relate this information to function (Dunlop *et al.*, 2005; Fraser *et al.*, 2009; Fraser & Jackson, 2011; Keedy *et al.*, 2015), and recent technical and methodological advances in data collection indicated that high-temperature X-ray data collection is possible but further developments are required to achieve the high resolutions needed to obtain ensemble information at temperatures above room temperature (Rajendran *et al.*, 2011).

Here we have developed and demonstrated a robust method for collecting high-quality X-ray diffraction data across physiological temperatures at a synchrotron beamline from single crystals, and we provide evidence for its potentially wide applicability. We collected high-resolution X-ray diffraction data of very high quality in the 293–363 K temperature range from proteinase K, thaumatin and lysozyme crystals. This is the first time, to our knowledge, that data beyond 2.0 Å resolution have been collected above 333 K and that complete and high-resolution X-ray diffraction data sets have been collected at 363 K. Here we acquired high-resolution data (1–1.5 Å), but this approach is of broader utility as meaningful biological information at physiological temperatures can be obtained from crystals diffracting at high-to-moderate resolutions. For example, major side-chain alternative rotameric states and bound water molecules can be identified in data sets of resolutions of 2.5 Å or better (Wlodawer *et al.*, 2008; Lang *et al.*, 2010). Most importantly, the approach presented here will allow high-quality X-ray data to be obtained more routinely at physiological temperatures.

Our method was implemented at SSRL beamline 14-1 but can be readily implemented at other SSRL beamlines and other synchrotrons. The crystal annealer device to control temperature equilibration can be built and adapted to most beamline setups in a matter of days. Fast data collection can be achieved using either the Eiger 16M detector (in this work) (Casanas *et al.*, 2016) or the Pilatus 6M detector (Broennimann *et al.*, 2006) available at most synchrotrons (including at SSRL beamlines 9-2 and 12-2). The X-ray flux at BL14-1 (1.7×10^{11} photons s^{-1} at 10.5 keV) is rather standard for protein X-ray beamlines (http://biosync.rcsb.org/), and larger beams required to match larger crystals are achievable by adjusting the X-ray optic instruments.

The method described herein is complementary to room-temperature serial femtosecond crystallography (SFX) at X-ray free-electron lasers (XFELs) and synchrotron-based serial synchrotron crystallography approaches that use microcrystals, with the advantage of potentially delivering higher resolutions from single crystals and excluding potentially complicating effects from non-isomorphous multi-crystal averaging. It is also advantageous given the limited XFEL facilities beam time availability, and the relatively long collection and processing times required for SFX. However, compared with SFX, our method has the disadvantage of data sets not being completely radiation damage free. Nevertheless, recent research has indicated that radiation damage does not significantly impact the conformational heterogeneity in protein crystals at room temperature (Gotthard *et al.*, 2019; Russi *et al.*, 2017; Roedig *et al.*, 2016). In addition, data collection times can be further decreased to $\leq$1 s for a complete data set at beamlines with higher X-ray fluxes, allowing more data to be collected at high-demand high-performance synchrotron beamlines.

The ability to robustly and efficiently collect X-ray diffraction data from single crystals at and above room temperature and obtain high-quality diffraction data also opens new opportunities for structural biologists and protein biochemists. As an example, it may be possible to obtain experimental phasing information directly at room temperature. While currently room-temperature data are collected for proteins for which the structure has previously been solved at cryo-temperatures, experimentally solving and obtaining conformational heterogeneity information for a new structure in a single experiment will reduce experimental time and modeling efforts. Similarly, the ability to obtain accurate experimental phases directly at room temperature could also help remove potential bias carried over from molecular replacement models obtained at cryo-temperature. Our preliminary results indicate that the resulting diffraction data are of high enough quality to allow native (single-wavelength anomalous diffraction) phasing (manuscript in preparation), which provides additional evidence for the very high quality of the data obtained using this approach. The ability to obtain high-quality diffraction data at high temperatures, as developed and presented in this work, may also enable direct observation of atomic-level changes in structure and conformational heterogeneity that precede unfolding events in proteins.

Acknowledgements

The contents of this publication are solely the responsibility of the authors and do not necessarily represent the official views of NIH or NIGMS. We thank Lisa Dunn for beam time allocation and access. We also thank Henry van den Bedem, James Fraser, Tung-Chung Mou, Thomas Poulos, Dirk Zajonc and members of the Herschlag laboratory for helpful discussions and comments on the manuscript.

Funding information

The following funding of this work is acknowledged: National Science Foundation, Directorate for Biological Sciences

(grant No. MCB-1714723 to DH); Human Frontier Science Program (award to FY). Use of the Stanford Synchrotron Radiation Lightsource (SSRL), SLAC National Accelerator Laboratory, is supported by the US Department of Energy, Office of Science and Office of Basic Energy Sciences, under contract No. DE-AC02-76SF00515. The SSRL Structural Molecular Biology Program is supported by the DOE Office of Biological and Environmental Research and by the National Institutes of Health (NIH), National Institute of General Medical Sciences (NIGMS, P41GM103393).

References

Atakisi, H., Moreau, D. W. & Thorne, R. E. (2018). *Acta Cryst.* D**74**, 264–278.
Bedem, H. van den, Dhanik, A., Latombe, J.-C. & Deacon, A. M. (2009). *Acta Cryst.* D**65**, 1107–1117.
Berg, J. M., Tymoczko, J. L., Stryer, L., Berg, J. M., Tymoczko, J. L. & Stryer, L. (2002). *Biochemistry*. New York: W. H. Freeman.
Blundell, T. L. & Johnson, L. N. (1976). *Protein Crystallography*. London: Academic Press.
Brändén, C.-I. & Tooze, J. (1999). *Introduction to Protein Structure*. New York: Taylor & Francis.
Broennimann, Ch., Eikenberry, E. F., Henrich, B., Horisberger, R., Huelsen, G., Pohl, E., Schmitt, B., Schulze-Briese, C., Suzuki, M., Tomizaki, T., Toyokawa, H. & Wagner, A. (2006). *J. Synchrotron Rad.* **13**, 120–130.
Brönnimann, C., Eikenberry, E. F., Horisberger, R., Hülsen, G., Schmitt, B., Schulze-Briese, C. & Tomizaki, T. (2003). *Nucl. Instrum. Methods Phys. Res. A*, **510**, 24–28.
Bury, C. S., Brooks-Bartlett, J. C., Walsh, S. P. & Garman, E. F. (2018). *Protein Sci.* **27**, 217–228.
Casanas, A., Warshamanage, R., Finke, A. D., Panepucci, E., Olieric, V., Nöll, A., Tampé, R., Brandstetter, S., Förster, A., Mueller, M., Schulze-Briese, C., Bunk, O. & Wang, M. (2016). *Acta Cryst.* D**72**, 1036–1048.
Dauter, Z. (1999). *Acta Cryst.* D**55**, 1703–1717.
Dauter, Z. (2017). *Protein Crystallography: Methods and Protocols*, edited by A. Wlodawer, Z. Dauter & M. Jaskolski, pp. 165–184. New York: Springer.
Dauter, Z. & Wlodawer, A. (2015). *Acta Cryst.* D**71**, 2217–2226.
Diederichs, K. (2010). *Acta Cryst.* D**66**, 733–740.
Dunlop, K. V., Irvin, R. T. & Hazes, B. (2005). *Acta Cryst.* D**61**, 80–87.
Elias, M., Wieczorek, G., Rosenne, S. & Tawfik, D. S. (2014). *Trends Biochem. Sci.* **39**, 1–7.
Evans, P. (2006). *Acta Cryst.* D**62**, 72–82.
Evans, P. R. & Murshudov, G. N. (2013). *Acta Cryst.* D**69**, 1204–1214.
Feller, G. (2010). *J. Phys. Condens. Matter*, **22**, 323101.
Fersht, A. (2017). *Structure and Mechanism in Protein Science: A Guide to Enzyme Catalysis and Protein Folding*. Singapore: World Scientific.
Fields, P. A., Dong, Y., Meng, X. & Somero, G. N. (2015). *J. Exp. Biol.* **218**, 1801–1811.
Fischer, M., Shoichet, B. K. & Fraser, J. S. (2015). *ChemBioChem*, **16**, 1560–1564.
Fraser, J. S., van den Bedem, H., Samelson, A. J., Lang, P. T., Holton, J. M., Echols, N. & Alber, T. (2011). *Proc. Natl Acad. Sci. USA*, **108**, 16247–16252.
Fraser, J. S., Clarkson, M. W., Degnan, S. C., Erion, R., Kern, D. & Alber, T. (2009). *Nature*, **462**, 669–673.
Fraser, J. S. & Jackson, C. J. (2011). *Cell. Mol. Life Sci.* **68**, 1829–1841.
Furnham, N., Blundell, T. L., DePristo, M. A. & Terwilliger, T. C. (2006). *Nat. Struct. Mol. Biol.* **13**, 184–185.
Garman, E. F. (2010). *Acta Cryst.* D**66**, 339–351.
Garman, E. F. & Owen, R. L. (2006). *Acta Cryst.* D**62**, 32–47.
Garman, E. F. & Weik, M. (2017). *J. Synchrotron Rad.* **24**, 1–6.
Gotthard, G., Aumonier, S., De Sanctis, D., Leonard, G., von Stetten, D. & Royant, A. (2019). *IUCrJ*, **6**, 665–680.
Halle, B. (2004). *Proc. Natl Acad. Sci. USA*, **101**, 4793–4798.
Henderson, R. & Clarke, B. C. (1990). *Proc. R. Soc. London Ser. B*, **241**, 6–8.
Holton, J. M. (2009). *J. Synchrotron Rad.* **16**, 133–142.
Hope, H. (1988). *Acta Cryst.* B**44**, 22–26.
Hope, H. (1990). *Annu. Rev. Biophys. Biophys. Chem.* **19**, 107–126.
Howells, M. R., Beetz, T., Chapman, H. N., Cui, C., Holton, J. M., Jacobsen, C. J., Kirz, J., Lima, E., Marchesini, S., Miao, H., Sayre, D., Shapiro, D. A., Spence, J. C. H. & Starodub, D. (2009). *J. Electron Spectrosc. Relat. Phenom.* **170**, 4–12.
Huang, P.-S., Boyken, S. E. & Baker, D. (2016). *Nature*, **537**, 320–327.
Juers, D. H. & Matthews, B. W. (2001). *J. Mol. Biol.* **311**, 851–862.
Kabsch, W. (2010). *Acta Cryst.* D**66**, 125–132.
Keedy, D. A., van den Bedem, H., Sivak, D. A., Petsko, G. A., Ringe, D., Wilson, M. A. & Fraser, J. S. (2014). *Structure*, **22**, 899–910.
Keedy, D. A., Hill, Z. B., Biel, J. T., Kang, E., Rettenmaier, T. J., Brandão-Neto, J., Pearce, N. M., von Delft, F., Wells, J. A. & Fraser, J. S. (2018). *eLife*, **7**, e36307.
Keedy, D. A., Kenner, L. R., Warkentin, M., Woldeyes, R. A., Hopkins, J. B., Thompson, M. C., Brewster, A. S., Van Benschoten, A. H., Baxter, E. L., Uervirojnangkoorn, M., McPhillips, S. E., Song, J., Alonso-Mori, R., Holton, J. M., Weis, W. I., Brunger, A. T., Soltis, S. M., Lemke, H., Gonzalez, A., Sauter, N. K., Cohen, A. E., van den Bedem, H., Thorne, R. E. & Fraser, J. S. (2015). *eLife*, **4**, e07574.
Kiefersauer, R., Than, M. E., Dobbek, H., Gremer, L., Melero, M., Strobl, S., Dias, J. M., Soulimane, T. & Huber, R. (2000). *J. Appl. Cryst.* **33**, 1223–1230.
Kuhlman, B. & Bradley, P. (2019). *Nat. Rev. Mol. Cell Biol.* **20**, 681–697.
Kurinov, I. V. & Harrison, R. W. (1995). *Acta Cryst.* D**51**, 98–109.
Lang, P. T., Ng, H.-L., Fraser, J. S., Corn, J. E., Echols, N., Sales, M., Holton, J. M. & Alber, T. (2010). *Protein Sci.* **19**, 1420–1431.
Marks, D. S., Hopf, T. A. & Sander, C. (2012). *Nat. Biotechnol.* **30**, 1072–1080.
McPhillips, T. M., McPhillips, S. E., Chiu, H.-J., Cohen, A. E., Deacon, A. M., Ellis, P. J., Garman, E., Gonzalez, A., Sauter, N. K., Phizackerley, R. P., Soltis, S. M. & Kuhn, P. (2002). *J. Synchrotron Rad.* **9**, 401–406.
Mora, E. de la, Coquelle, N., Bury, C. S., Rosenthal, M., Holton, J. M., Carmichael, I., Garman, E. F., Burghammer, M., Colletier, J.-P. & Weik, M. (2020). *Proc. Natl Acad. Sci. USA*, **117**, 4142–4151.
Nave, C. & Garman, E. F. (2005). *J. Synchrotron Rad.* **12**, 257–260.
Owen, R. L., Axford, D., Nettleship, J. E., Owens, R. J., Robinson, J. I., Morgan, A. W., Doré, A. S., Lebon, G., Tate, C. G., Fry, E. E., Ren, J., Stuart, D. I. & Evans, G. (2012). *Acta Cryst.* D**68**, 810–818.
Owen, R. L., Paterson, N., Axford, D., Aishima, J., Schulze-Briese, C., Ren, J., Fry, E. E., Stuart, D. I. & Evans, G. (2014). *Acta Cryst.* D**70**, 1248–1256.
Owen, R. L., Rudiño-Piñera, E. & Garman, E. F. (2006). *Proc. Natl Acad. Sci. USA*, **103**, 4912–4917.
Paithankar, K. S., Owen, R. L. & Garman, E. F. (2009). *J. Synchrotron Rad.* **16**, 152–162.
Petsko, G. A. (1996). *Nat. Struct. Mol. Biol.* **3**, 565–566.
Pflugrath, J. W. (2015). *Acta Cryst.* F**71**, 622–642.
Rajendran, C., Dworkowski, F. S. N., Wang, M. & Schulze-Briese, C. (2011). *J. Synchrotron Rad.* **18**, 318–328.
Ringe, D. & Petsko, G. A. (1985). *Prog. Biophys. Mol. Biol.* **45**, 197–235.
Roedig, P., Duman, R., Sanchez-Weatherby, J., Vartiainen, I., Burkhardt, A., Warmer, M., David, C., Wagner, A. & Meents, A. (2016). *J. Appl. Cryst.* **49**, 968–975.
Russi, S., González, A., Kenner, L. R., Keedy, D. A., Fraser, J. S. & van den Bedem, H. (2017). *J. Synchrotron Rad.* **24**, 73–82.
Sanchez-Weatherby, J., Bowler, M. W., Huet, J., Gobbo, A., Felisaz, F., Lavault, B., Moya, R., Kadlec, J., Ravelli, R. B. G. & Cipriani, F. (2009). *Acta Cryst.* D**65**, 1237–1246.

Sandalova, T., Schneider, G., Käck, H. & Lindqvist, Y. (1999). *Acta Cryst.* D**55**, 610–624.
Siddiqui, K. S. & Cavicchioli, R. (2006). *Annu. Rev. Biochem.* **75**, 403–433.
Sjögren, T., Carlsson, G., Larsson, G., Hajdu, A., Andersson, C., Pettersson, H. & Hajdu, J. (2002). *J. Appl. Cryst.* **35**, 113–116.
Skrzypczak-Jankun, E., Bianchet, M. A., Mario Amzel, L. & Funk, M. O. (1996). *Acta Cryst.* D**52**, 959–965.
Southworth-Davies, R. J., Medina, M. A., Carmichael, I. & Garman, E. F. (2007). *Structure*, **15**, 1531–1541.
Thomaston, J. L., Woldeyes, R. A., Nakane, T., Yamashita, A., Tanaka, T., Koiwai, K., Brewster, A. S., Barad, B. A., Chen, Y., Lemmin, T., Uervirojnangkoorn, M., Arima, T., Kobayashi, J., Masuda, T., Suzuki, M., Sugahara, M., Sauter, N. K., Tanaka, R., Nureki, O., Tono, K., Joti, Y., Nango, E., Iwata, S., Yumoto, F., Fraser, J. S. & DeGrado, W. F. (2017). *Proc. Natl Acad. Sci. USA*, **114**, 13357–13362.
Tilton, R. F., Dewan, J. C. & Petsko, G. A. (1992). *Biochemistry*, **31**, 2469–2481.
Ufimtsev, I. S. & Levitt, M. (2019). *Proc. Natl Acad. Sci. USA*, **116**, 10813–10818.
Warkentin, M., Badeau, R., Hopkins, J. B., Mulichak, A. M., Keefe, L. J. & Thorne, R. E. (2012). *Acta Cryst.* D**68**, 124–133.
Warkentin, M., Badeau, R., Hopkins, J. & Thorne, R. E. (2011). *Acta Cryst.* D**67**, 792–803.
Warkentin, M. & Thorne, R. E. (2010). *Acta Cryst.* D**66**, 1092–1100.
Wlodawer, A., Minor, W., Dauter, Z. & Jaskolski, M. (2008). *FEBS J.* **275**, 1–21.
Woldeyes, R. A., Sivak, D. A. & Fraser, J. S. (2014). *Curr. Opin. Struct. Biol.* **28**, 56–62.
Zeldin, O. B., Gerstel, M. & Garman, E. F. (2013). *J. Appl. Cryst.* **46**, 1225–1230.